Quantum electron transport in magnetically entangled subbands

William Mayer and Sergey Vitkalov*
Physics Department, City College of the City University of New York, New York 10031, USA

A. A. Bykov
A. V. Rzhanov Institute of Semiconductor Physics, Novosibirsk 630090, Russia
and Physics Department, Novosibirsk State University, Novosibirsk 630090, Russia
(Received 6 March 2017; revised manuscript received 2 May 2017; published 28 July 2017)

Transport properties of highly mobile two-dimensional (2D) electrons in symmetric GaAs quantum wells with two populated subbands placed in tilted magnetic fields are studied at high temperatures. Quantum positive magnetoresistance (QPMR) and magneto-intersubband resistance oscillations (MISO) are observed in quantizing magnetic fields, $B_\perp$, applied perpendicular to the 2D layer. QPMR displays contributions from electrons with considerably different quantum lifetimes, $\tau_q^{(1,2)}$, confirming the presence of two subbands in the studied system. MISO evolution with $B_\perp$ agrees with the obtained quantum scattering times only if an additional reduction of the MISO magnitude is applied at small magnetic fields. This indicates the presence of a yet unknown mechanism leading to MISO damping. Application of an in-plane magnetic field produces a strong decrease of both QPMR and MISO magnitude. The reduction of QPMR is explained by spin splitting of Landau levels indicating a g factor, $g \approx 0.4$, which is considerably less than the g factor found in GaAs quantum well with a single subband populated. In contrast to QPMR, the decrease of MISO magnitude is largely related to the in-plane magnetic field induced entanglement between quantum levels in different subbands that, in addition, increases the MISO period.

DOI: 10.1103/PhysRevB.96.045436

I. INTRODUCTION

The orbital quantization of electron trajectories and spectrum in magnetic fields significantly affects the electron transport in condensed materials [1,2]. Spin degrees of freedom further enrich the electron response [3]. Shubnikov–de Haas (SdH) resistance oscillations [1] and the quantum Hall effect (QHE) [4] are famous examples of the quantization effect on electron transport at temperatures T less than the energy $\Delta_c = \hbar\omega_c$ separating Landau levels. Here ω_c is the cyclotron frequency. At high temperatures $T \gg \hbar\omega_c$, SdH oscillations are absent due to the spectral averaging of the oscillating density of states (DOS) in the energy interval $\delta\epsilon \sim T$ near the Fermi energy E_F. In this high temperature regime other quantum effects exist.

Two-dimensional electron systems with multiple populated subbands exhibit additional quantum resistance oscillations [5–10]. These magneto-intersubband oscillations (MISO) of the resistance are due to an alignment between Landau levels from different subbands i and j with corresponding energies E_i and E_j. Resistance maxima occur at magnetic fields at which the gap between the bottoms of subbands, $\Delta_{ij} = E_i - E_j$, equals a multiple of the Landau level spacing, $\hbar\omega_c$: $\Delta_{ij} = k\hbar\omega_c$, where k is an integer [11–14]. At this condition electron elastic scattering on impurities is enhanced due to the possibility of electron transitions between the aligned quantum levels of the ith and jth subbands. At magnetic fields corresponding to the condition $\Delta_{ij} = (k + 1/2)\hbar\omega_c$ the intersubband electron scattering is suppressed. This spectral overlap between two subbands oscillates with the magnetic field and leads to MISO, which are periodic in the inverse magnetic field. In contrast to SdH oscillations, MISO are significantly less sensitive to temperature and exist at $kT \gg \hbar\omega_c$.

Recently MISO in wide (56 nm) GaAs quantum wells with three subbands populated were investigated in tilted magnetic fields [15]. An application of in-plane magnetic field produces dramatic changes in MISO and the corresponding electron spectrum. Three regimes have been identified. At $\hbar\omega_c \ll \Delta_{12}$, the in-plane magnetic field increases considerably the gap Δ_{12}, which is consistent with the semiclassical regime of electron propagation. In contrast, at strong magnetic fields $\hbar\omega_c \gg \Delta_{12}$ relatively weak oscillating variations of the electron spectrum with the in-plane magnetic field have been observed. At $\hbar\omega_c \approx \Delta_{12}$, the electron spectrum undergoes a transition between these two regimes through magnetic breakdown [16–24]. In this transition regime MISO with odd quantum number k terminate, while MISO corresponding to even k evolve continuously into the high-field regime corresponding to $\hbar\omega_c \gg \Delta_{12}$. The observed results are found to be in an excellent agreement with the theory [22], considering the wide quantum well to be two parallel two-dimensional (2D) electron systems coupled by a tunneling with an amplitude t_0 through a barrier of width d. The observed complex behavior of MISO in the tilted magnetic field was quantitatively understood in the terms of the entanglement of the orbital electron motion in different subbands induced by the in-plane magnetic field. Indeed, due to the in-plane magnetic field each level of a subband interacts directly with two levels of another subband, leading to an entangled mesh of the couplings between quantum levels [15]. No effects of electron spin degree of freedom were detected in this study.

With a decrease of the width of a quantum well, the gap Δ_{12} increases. At $\Delta_{12} > E_F$ only a single subband is populated in the quantum well. These quantum wells do

*Corresponding author: svitkalov@ccny.cuny.edu

not demonstrate MISO but continue to display a quantum positive magnetoresistance (QPMR). This effect is due to enhanced electron scattering on impurities that results from the increasing amplitude of the electron wave function in stronger magnetic fields. The latter is a direct consequence of the reduction of the electron orbit (size of the wave function) with $B_\perp$. QPMR is in some respect similar to MISO and reflects the enhancement of the intrasubband impurity scattering due to the quantization of the electron spectrum [13,14,25]. QPMR has been observed in electron systems with two populated subbands [26] and in narrow (13 nm) quantum wells with a single subband populated [27]. The later was recently investigated in tilted magnetic fields [28]. These investigations have demonstrated that the QPMR magnitude decreases significantly with application of an in-plane magnetic field. The QPMR decrease is found to be strongly correlated with the reduction of SdH amplitude, indicating the spin origin of the effect. This considerable effect of the spin degree of freedom on the electron-impurity scattering was unexpected, since it is widely accepted that in GaAs high mobility quantum wells most impurities are not magnetic.

In the present paper we report a study of transport properties of high quality GaAs quantum wells of an intermediate width, $d_0 = 26$ nm. The goals of this study are to detect effects of the spin degree of freedom on MISO, which have not been seen, as well as to investigate the effect of the spin splitting on QPMR [28] in a 2D system with two subbands populated. Experiments presented below demonstrate a significant reduction of the QPMR with the application of the in-plane magnetic field, which is in good agreement with the modification of the electron spectrum via the Zeeman effect with g factor $g \approx 0.43 \pm 0.07$. The observed g factor is, however, significantly less than the enhanced electron g factor observed in GaAs quantum wells with a single subband populated.

MISO also have demonstrated a strong reduction of magnitude with the in-plane magnetic field. However, in contrast to the QPMR decrease, the MISO reduction is found to be predominantly related to a modification of the electron spectrum via the orbital coupling of two subbands induced by the in-plane magnetic field. The Zeeman term provides a subleading contribution to the MISO reduction. The in-plane magnetic field induced entanglement between wave functions in two subbands also leads to variations of MISO period which are found to be in good agreement with our experiments. This agreement provides the basis for a new method to measure the width of quantum wells.

At small magnetic fields MISO indicate the presence of a yet unknown mechanism of additional damping. We found that a quite small nonparabolicity of the electron spectrum could explain the additional MISO damping at zero in-plane magnetic field. However an overly strong reduction of the numerically computed MISO amplitude with the magnetic field tilt does not allow us to firmly identify the nonparabolicity of the electron spectrum as the only cause of the observed additional MISO decrease.

Finally a cross-comparison of QPMR and classical magnetoresistance in perpendicular magnetic fields shows good mutual agreement with the quantitative theory [14,25,29] and indicates the dominant contribution of the intersubband impurity scattering to the electron transport. An analysis of the MISO amplitude shows significantly less effect of the scattering between subbands, which destroys the overall agreement with theory.

II. EXPERIMENTAL SETUP

The studied GaAs quantum wells were grown by molecular beam epitaxy on a semi-insulating (001) GaAs substrate. The material was fabricated from a selectively doped GaAs single quantum well of width $d_0 = 26$ nm sandwiched between AlAs/GaAs superlattice barriers. The studied samples were etched in the shape of a Hall bar. The width and the length of the measured part of the samples are $W = 50\,\mu$m and $L = 250\,\mu$m. AuGe eutectic was used to provide electric contacts to the 2D electron gas. Two samples were studied at temperature 4.2 kelvin in magnetic fields up to 9 tesla applied *in situ* at different angle α relative to the normal to 2D layers and perpendicular to the applied current. The angle α was evaluated using the Hall voltage $V_H = B_\perp/(en_T)$, which is proportional to the perpendicular component, $B_\perp = B\cos(\alpha)$, of the total magnetic field B. The total electron density of sample N1, $n_T \approx 7.97 \times 10^{11}$ cm^{-2}, was evaluated from the Hall measurements taken at $\alpha = 0^\circ$ in classically strong magnetic fields [30]. An average electron mobility $\mu \approx 1.2 \times 10^6$ cm^2/V s was obtained from n_T and the zero-field resistivity. An analysis of the periodicity of MISO in the inverse magnetic field yields the gap $\Delta_{12} = 15.15$ meV between bottoms of the conducting subbands, Fermi energy $E_F = 21.83$ meV, and electron densities $n_1 = 6.1 \times 10^{11}$ cm^{-2} and $n_2 = 1.87 \times 10^{11}$ cm^{-2} in the two populated subbands. Sample N2 had density $n_T \approx 8.6 \times 10^{11}$ cm^{-2}, mobility $\mu \approx 1.0 \times 10^6$ cm^2/V s, and the gap $\Delta_{12} = 15.10$ meV. Both samples demonstrated very similar quantum electron transport in magnetic fields. Below we present data for sample N1.

Sample resistance was measured using the four-point probe method. We applied a 133 Hz ac excitation of $I_{ac} = 1\ \mu$A through the current contacts and measured the longitudinal (in the direction of the electric current, x direction) and Hall ac (along the y direction) voltages (V_{xx}^{ac} and V_H^{ac}) using two lock-in amplifiers with 10 MΩ input impedances. The measurements were done in the linear regime in which the voltages are proportional to the applied current.

III. EXPERIMENTAL RESULTS

Figure 1 presents dependences of the dissipative resistance of 2D electrons on the perpendicular magnetic field $B_\perp$, taken at different angles α between the direction of the total magnetic field $\vec{B}$ and the normal to the 2D layer. At $\alpha = 0$ degrees and $B_\perp < 0.025$ T the magnetoresistance demonstrates a small increase related to classical magnetoresistance [14,26,29–31]. At a higher magnetic field the magnetoresistance slowly increases, oscillating at $B_\perp > 0.07$ T. These oscillations are MISO. MISO maxima correspond to the condition

$$\Delta_{12} = j\hbar\omega_c, \tag{1}$$

where $\Delta_{12} = E_2 - E_1$ is the energy difference between bottoms of two occupied subbands and the index j is a positive integer [13,14]. At even higher magnetic fields ($\hbar\omega_c > kT$, corresponding to $B_\perp > 0.4$ tesla at $T = 4.2$ K) there are SdH

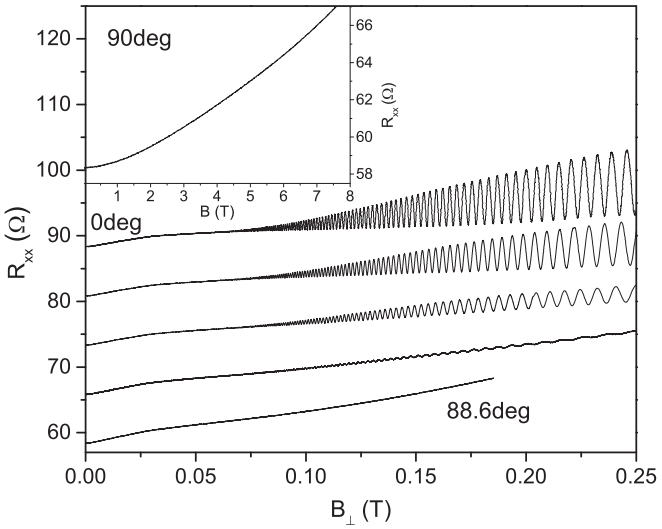

FIG. 1. Dependence of the dissipative resistance R_{xx} of 2D electrons on a perpendicular magnetic field taken at different angles $\alpha = 0$, 86, 87, 88.1, and 88.6 degrees between magnetic field B and the normal to the 2D layer. Curves at angles $\alpha < 88.6$ degrees are shifted up for clarity. The inset shows magnetoresistance in a parallel magnetic field.

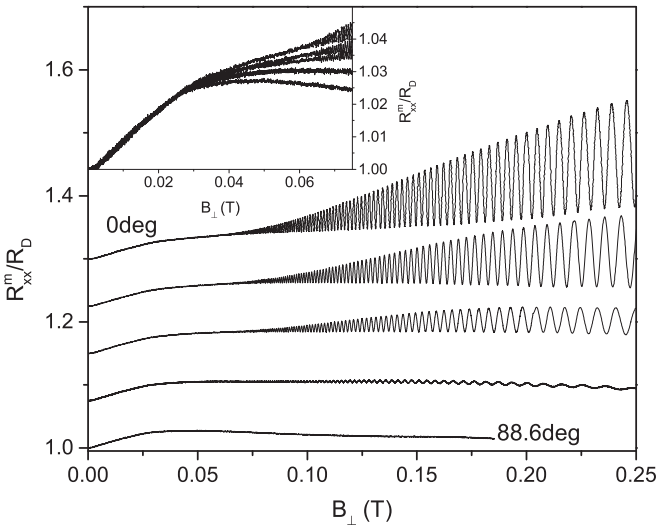

FIG. 2. Magnetic field dependence of the normalized resistance without the effect of the parallel magnetic field on the resistance presented in the inset in Fig. 1. The $B_\parallel$ contribution is subtracted numerically from the curves shown in Fig. 1. Obtained curves are offset for clarity. The inset presents the same curves without offset. At $B_\perp < 0.025$ T the inset demonstrates classical magnetoresistance in two subband systems that is independent of the angle α while at $B_\perp > 0.025$ T progressive deviation between curves at different angles is observed and related to the quantum positive magnetoresistance.

oscillations (not shown). In this paper we focus on the low magnetic field (high temperature) regime, $\hbar\omega_c \ll kT$, where SdH oscillations are absent.

The most observable property of the angular evolution of the magnetoresistance is the significant reduction of MISO amplitude at high angles α. Another striking effect is a variation of the MISO frequency with angle α, which can be seen by a comparison of the maximum positions at high $B_\perp$. Other variations of the magnetoresistance are less obvious and required more accurate comparison.

The inset in Fig. 1 presents the dependence of the resistance on magnetic field B which is parallel to the 2D electron layer. The in-plane magnetic field of 8 T increases the resistance by 10–15 percent. This small increase occurs at $B_\perp = 0$ T and, thus, is not relevant to the quantization of the electron motion and spectrum induced by the perpendicular magnetic field. This in-plane magnetoresistance is driven by a mechanism that is different from the Landau quantization leading to MISO and QPMR. Since observed quantum contributions to the resistivity (QPMR and MISO) are relatively small, it makes sense to expect that an application of the perpendicular magnetic field may provide a very small contribution (if any) to the observed small in-plane magnetoresistance. Below we assume that the magnetoresistance shown in the inset in-plane does not depend on the perpendicular magnetic field.

Using this assumption, we have subtracted numerically the contribution of the in-plane magnetic field from the original experimental data shown in Fig. 1. Figure 2 presents the result of the subtraction normalized by the resistance at zero magnetic field, $R_D = R_{xx}(B = 0T)$. The modified resistance, R^m_{xx}, is computed using the following formula: $R^m_{xx}(B_\perp) = R_{xx}(B_\perp) - R^\parallel_{xx}(B_\parallel)$, where $R^\parallel_{xx}$ is the in-plane magnetoresistance shown in the inset in Fig. 1 and $B_\parallel = \tan(\alpha)B_\perp$ is the in-plane magnetic field applied to the sample.

The applied procedure yields an observable effect on the dependencies at large angles at which $B_\parallel$ is large. In particular, the modified magnetoresistance R^m_{xx} at $\alpha = 88.6$ degrees decreases with the perpendicular field, while the original dependence does increase at $B_\perp > 0.05$ T. The most impressive outcomes of the applied procedure are the collapse of the classical magnetoresistance obtained at different angles in perpendicular magnetic fields below 0.025 T and the progressive decrease of the magnetoresistance with the angle at $B_\perp > 0.025$ T. This is shown in the inset in Fig. 2. Both outcomes are very similar to the ones obtained in 2D electron systems with a single subband populated [28]. Below we analyze quantitatively the angular evolution of the oscillating (MISO) and nonoscillating (related to QPMR) contents of the magnetoresistance.

Figure 3(a) presents the nonoscillating content of the normalized magnetoresistance, R^*_{QPMR}/R_D, obtained at different angles in a broad range of perpendicular magnetic fields. The noticeable property of the obtained angular evolution is the fact that angular variations of the electron transport start quite sharply at $B_\perp \approx 0.025$ T at which the classical magnetoresistance starts to saturate, indicating the regime of the classically strong magnetic fields [29,30]: $\omega_c\tau_{tr} \gg 1$, where τ_{tr} is the transport scattering time. This result agrees with the beginning of the quantization of the electron motion, $\omega_c\tau_q \sim 1$, since in the studied system a small angle scattering dominates: $\tau_q \ll \tau_{tr}$ [32].

The angular variations of the nonoscillating content of the magnetoresistance at $B_\perp > 0.025$ T are related to the angular evolution of the quantized electron spectrum leading to QPMR. Figure 3(a) shows progressively stronger angular

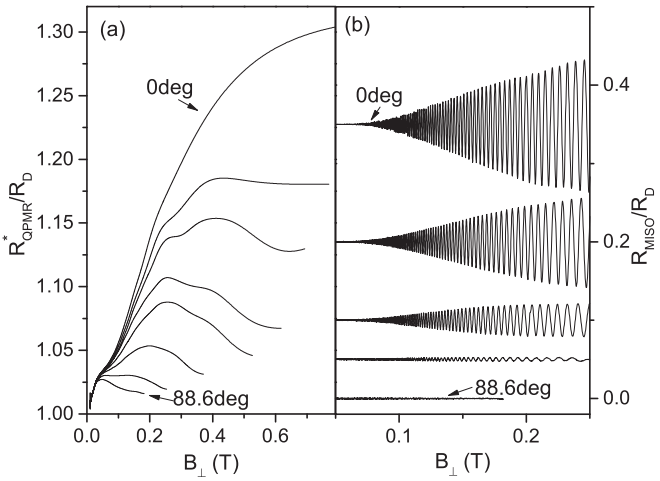

FIG. 3. Figure (a) shows nonoscillating content of magnetoresistance related to QPMR at various angles. From the top to the bottom $\alpha = 0, 80, 82.5, 85, 86, 87, 88.1$, and 88.6 degrees. Figure (b) presents oscillating content of the magnetoresistance at the same set of angles as in Figs. 1 and 2.

variations of QPMR at higher $B_\perp$. This is in agreement with the progressively stronger quantization of the electron spectrum at higher $B_\perp$. We have found that the strong increase of the angular variations of QPMR with $B_\perp$ is in good quantitative agreement with the model presented below. The comparison between the experiment and model has revealed that the dominant mechanism leading to the angular decrease of QPMR is spin (Zeeman) splitting of Landau levels in magnetic fields. This result agrees with the one obtained in systems with a single populated subband [28].

Figure 3(b) presents the oscillating content of the magnetoresistance, which is related to MISO. The figure shows strong decrease of MISO at high angles. In contrast to the angular variations of QPMR presented below, quantitative analysis indicates that the angular variations of MISO are predominantly due to the modifications of the electron spectrum via an entanglement of the electron orbital states induced by the in-plane magnetic field. The observed spin contribution to the decrease of the MISO amplitude is subdominant. Below we present a theoretical framework describing the angular evolution of quantum electron transport.

IV. MODEL OF QUANTUM ELECTRON TRANSPORT

A microscopic description of both QPMR and MISO in perpendicular magnetic fields (at $\alpha = 0^\circ$) is presented in papers [13,14,25] neglecting any spin related effects in particular the Zeeman term. An account of the Zeeman splitting for QPMR is proposed in Ref. [28] for 2D systems with a single subband populated. The proposed model utilizes a similarity of QPMR and magneto-intersubband resistance oscillations (MISO) [5,6,13–15]. The model considers two spin subbands shifted with respect to each other by the Zeeman effect. In each spin subband the energy spectrum evolves in accordance with Landau quantization. A scattering assisted spin mixing between different subbands is postulated to provide the correlation between the angular evolutions of SdH oscillations and QPMR observed in the experiment [28]. Within this model the absence of the scattering between spin subbands would lead to the absence of an angular evolution of the QPMR associated with the Zeeman effect, in contrast to the angular dependence of SdH oscillations. The origin of the spin mixing requires further investigations.

A mixing between different spin subbands has been reported in Si metal-oxide-semiconductor field-effect transistors (MOSFETs) [33]. The experiments show sizable contributions of the product of spin-up and spin-down density of states to quantum resistance oscillations. Furthermore, investigations of the resistivity tensor in tilted magnetic fields have revealed an independence of the Hall coefficient on the spin subband populations while the electron mobility in each spin subband was substantially affected by the in-plane magnetic field [34]. This behavior has been interpreted as a mixing between spin subbands due to electron-electron interaction [35]. Spin-orbit coupling can also provide a mixing via local impurity scattering [3,28].

In this section the recent model [28], describing the angular evolution of QPMR in 2D electron systems with a single populated subband, is generalized to 2D systems with two populated subbands. The spatial subbands are the result of quantization of the electron wave function in the z direction. The z axis is perpendicular to the 2D electron layer (x-y directions) of a width d. Index $i = 1$ (2) labels the low (high) subband with the energy E_1 (E_2) at the subband bottom. The subband separation is $\Delta_{12} = E_2 - E_1$.

A. Response in perpendicular magnetic field, $B_\parallel = 0$

At the beginning we consider the magnetic field applied perpendicularly to 2D electron systems ($\alpha = 0$ degrees). In the simplest case of small quantizing magnetic fields $\omega_c\tau_q < 1$, the main contribution to both MISO and QPMR comes from the fundamental harmonic of quantum oscillations of the density of states (DOS) corresponding to spin-up ($\uparrow$) and spin-down ($\downarrow$) subbands. The DOS of the ith spatial subband, $\nu_i(\epsilon)$, reads [2,28]

$$\frac{\nu_1(\epsilon \geqslant 0)}{\nu_0} = \left[1 - 2\delta_1 \cos\left(\frac{2\pi\epsilon}{\hbar\omega_c}\right)\cos\left(\frac{\pi\Delta_Z^{(1)}}{\hbar\omega_c}\right)\right],$$
$$\frac{\nu_2(\epsilon \geqslant \Delta_{12})}{\nu_0} = \left[1 - 2\delta_2 \cos\left(\frac{2\pi(\epsilon - \Delta_{12})}{\hbar\omega_c}\right)\cos\left(\frac{\pi\Delta_Z^{(2)}}{\hbar\omega_c}\right)\right], \quad (2)$$

where $\nu_0 = m/(\pi\hbar^2)$ is the DOS at zero magnetic field, $\delta_i = \exp(-\pi/\omega_c\tau_q^{(i)})$ is the Dingle factor, $\Delta_Z^{(i)} = \mu g_i B$ is the Zeeman splitting, and $\tau_q^{(i)}$ is the quantum scattering time in the ith subbands.

The 2D conductivity σ is obtained from the following relation:

$$\sigma(B) = \int d\epsilon\, \sigma(\epsilon)\left(-\frac{\partial f}{\partial\epsilon}\right). \quad (3)$$

The integral is an average of the conductivity $\sigma(\epsilon)$ taken essentially for energies ϵ inside the temperature interval kT near the Fermi energy, where $f(\epsilon)$ is the electron distribution function at a temperature T [2].

The following expression approximates the conductivity $\sigma(\epsilon)$ at small quantizing magnetic fields:

$$\sigma(\epsilon) = \sigma_D^{(1)}\tilde{\nu}_1(\epsilon)^2 + \sigma_D^{(2)}\tilde{\nu}_2(\epsilon)^2 + \sigma_D^{(12)}\tilde{\nu}_1(\epsilon)\tilde{\nu}_2(\epsilon), \quad (4)$$

where $\tilde{\nu}_i(\epsilon) = \nu_i(\epsilon)/\nu_0$ are normalized total densities of states in each spatial subband. Parameters $\sigma_D^{(1)}(B_\perp)$ and $\sigma_D^{(2)}(B_\perp)$ are Drude like conductivities related to contributions of an effective intrasubband scattering, while the factor $\sigma_D^{(12)}(B_\perp)$ accounts contributions of the inter-subband scattering [13,14].

The main assumption of this model is utilized in Eq. (4). Namely, the impurity scattering within a spin sector is considered to be comparable with the impurity scattering between spin-up and spin-down sectors, when the energies of the spin sectors are the same. In other words a spin up (spin-down) electron has equal probability to scatter into a spin-up or spin-down quantum state [28].

A substitution of Eqs. (4) and (2) into Eq. (3) yields the following relation for the conductivity:

$$\sigma(B) = \sigma_D + \sigma_{QPMR} + \sigma_{MISO}, \quad (5)$$

where $\sigma_D(B) = \sigma_D^{(1)} + \sigma_D^{(2)} + \sigma_D^{(12)}$ is the Drude (classical) conductivity in a magnetic field. The last two terms in Eq. (5) describe quantum contributions to the electron transport in the high temperature regime: $\hbar\omega_c \ll kT$. The term σ_{QPMR} describes quantum positive magnetoresistance:

$$\sigma_{QPMR} = 2\left[\sigma_D^{(1)}\delta_1^2\cos^2\left(\frac{\pi\Delta_Z^{(1)}}{\hbar\omega_c}\right) + \sigma_D^{(2)}\delta_2^2\cos^2\left(\frac{\pi\Delta_Z^{(2)}}{\hbar\omega_c}\right)\right]. \quad (6)$$

At $\Delta_Z = 0$, Eq. (6) reproduces QPMR in perpendicular magnetic fields [14,25,27].

The term σ_{MISO} is related to magneto-intersubband resistance oscillations:

$$\sigma_{MISO} = 2\sigma_D^{(12)}\delta_1\delta_2\cos\left(\frac{\pi\Delta_Z^{(1)}}{\hbar\omega_c}\right)\cos\left(\frac{\pi\Delta_Z^{(2)}}{\hbar\omega_c}\right) \times \cos\left(\frac{2\pi\Delta_{12}}{\hbar\omega_c}\right). \quad (7)$$

At $\Delta_Z^{(i)} = 0$, Eq. (7) reproduces MISO in perpendicular magnetic fields yielding Eq. (1) for MISO maxima [13,14].

B. Effect of in-plane magnetic field

With no in-plane magnetic field applied, the spatial subbands are coupled to each other via elastic scattering. An in-plane magnetic field, $B_\parallel$, provides an additional coupling via Lorentz force coming from the last term in Eq. (8). This additional $B_\parallel$ coupling preserves the degeneracy of the quantum levels but induces variations of the electron spectrum, which, due to a relativistic origin of Lorentz force, are dependent on the energy (velocity). These spectrum variations destroy the exact energy periodicity of the spectral overlap between different subbands existing at zero in-plane magnetic field and leading to MISO. In particular, in contrast to the $B_\parallel = 0$ T case, the energy independent condition for the MISO maximum presented by Eq. (1) is not relevant anymore since the intersections of the quantum levels of low and high subbands do not occur at the same perpendicular magnetic field if an in-plane magnetic field is applied.

To estimate this effect quantitatively we compute numerically the electron spectrum of an ideal two subband system in a tilted magnetic field, neglecting the impurity scattering. The impurity scattering is introduced then by a broadening of the bare quantum levels using the Gaussian shape of the DOS with the preserved level degeneracy. Finally, the conductivity is numerically evaluated via Eqs. (3) and (4) using the computed DOS.

In the comparison between the model and experiment, we found that the Zeeman effect provides a subleading contribution to the resistance. We did not find any indication of the dependence of the Zeeman splitting on the energy in the vicinity of Fermi energy. Our results are reasonably well described by an energy independent Zeeman term: $\Delta_Z^{(i)} = \mu g_i B$. Numerical computations of the electron spectrum start with a spinless Hamiltonian describing a 2D electron in a tilted magnetic field. The Zeeman term splits the obtained quantum levels. In the spectrum computations, spin-orbital interactions are neglected and the Zeeman term is assumed to be the same in both spatial subbands.

We consider a quantum well of a width d in the z direction formed by a rectangular electrostatic potential $V(z)$ with infinitely high walls and placed in a tilted magnetic field $\vec{B} = (-B_\parallel, 0, B_\perp)$. Electrons are described by the Hamiltonian [15]

$$H = \frac{\hbar^2 k_x^2}{2m^*} + \frac{e^2 B_\perp^2}{2m^*}x^2 + \frac{\hbar^2 k_z^2}{2m^*} + V(z) + \frac{e^2 B_\parallel^2}{2m^*}z^2 + \frac{e^2 B_\perp B_\parallel}{m^*}xz, \quad (8)$$

where m^* is electron effective mass. To obtain Eq. (8) we have used the gauge $(0, B_\perp x + B_\parallel z, 0)$ of the vector potential and applied the transformation $x \to x - \hbar k_y/eB_\perp$.

The first four terms of the Hamiltonian describe the 2D electron system in a perpendicular magnetic field. The corresponding eigenfunctions of the system are $|N,\xi\rangle$, where $N = 0,1,2,\ldots$ represents the Nth Landau level (the lateral quantization) and $\xi = \mathrm{S}, \mathrm{AS}$ describes the symmetric (S) and antisymmetric (AS) configurations of the wave function in the z direction (vertical quantization): $|N,S\rangle = |N\rangle(2/d)^{1/2}\cos(\pi z/d)$ and $|N,AS\rangle = |N\rangle(2/d)^{1/2}\sin(2\pi z/d)$.

Using functions $|N,\xi\rangle$ as the basis set, one can present the Hamiltonian in matrix form. The matrix contains four matrix blocks: $\hat{H} = (\hat{E}^S, \hat{T}; \hat{T}, \hat{E}^{AS})$, where the semicolon separates rows. The diagonal matrices, $\hat{E}^S$ and $\hat{E}^{AS}$, represent energy of the symmetric and antisymmetric wave functions in different orbital states N:

$$E_{mn}^S = \delta_{mn}\left[\hbar\omega_c\left((n-1)+\frac{1}{2}\right) + \frac{e^2 B_\parallel^2 d^2\left[\frac{1}{12} - \frac{1}{2\pi^2}\right]}{2m^*}\right],$$
$$E_{mn}^{AS} = \delta_{mn}\left[\hbar\omega_c\left((n-1)+\frac{1}{2}\right) + \Delta_{12} + \frac{e^2 B_\parallel^2 d^2\left[\frac{1}{12} - \frac{1}{8\pi^2}\right]}{2m^*}\right], \quad (9)$$

where $\Delta_{12} = E_2 - E_1$ is the energy difference between bottoms of two spatial subbands and indexes $m = 1,2,\ldots,N_{\max}$ and $n = 1,2,\ldots,N_{\max}$ enumerate rows and columns of the matrix, respectively. These indexes are related to the orbital number N: $n,m = N+1$, since the orbital number $N = 0,1,2,\ldots$. In numerical computations the maximum number $N_{\max}$ is chosen to be about twice larger than the orbital number N_F corresponding to Fermi energy E_F. Further increase of $N_{\max}$ show a very small (within 1%) deviation from the dependencies obtained at $N_{\max} \approx 2N_F$.

The first term in Eq. (9) describes the orbital quantization of electron motion. The last term in Eq. (9) describes diamagnetic shift of the quantum levels and is related to the fifth term in Eq. (8). In the basis set $|N,\xi\rangle$ the diamagnetic term is proportional to $\langle\xi|z^2|\xi\rangle$. The diamagnetic terms do not depend on N.

The off-diagonal matrix $\hat{T}$ is related to the last term in Eq. (8), which mixes symmetric and antisymmetric states. Since $x = l_{B\perp}(a^* + a)/\sqrt{2}$ includes the raising a^* and lowering a operators of the Landau orbits, the last term in Eq. (8) couples Landau levels with orbital numbers different by 1. Here $l_{B\perp} = (\hbar/eB_\perp)^{1/2}$ is the magnetic length in $B_\perp$. As a result, for $n > m$ the matrix element T_{mn} between states $|N,S\rangle$ and $|N+1,AS\rangle$ is

$$T_{mn} = \delta_{m+1,n}\frac{e^2 B_\parallel B_\perp l_{B\perp}}{m^*}\langle N|\frac{a^* + a}{\sqrt{2}}|N+1\rangle\langle S|z|AS\rangle$$
$$= \delta_{m+1,n}\hbar\omega_c\left[\frac{16B_\parallel d}{9\pi^2 B_\perp l_{B\perp}}\right](n/2)^{1/2}. \quad (10)$$

The matrix $\hat{T}$ is a symmetric matrix: $T_{mn} = T_{nm}$. The Hamiltonian $\hat{H}$ is diagonalized numerically at different magnetic fields $B_\perp$ and $B_\parallel$. To analyze the spectrum, the obtained eigenvalues of the Hamiltonian are enumerated in ascending order using positive integer index $l = 1,2,\ldots$. Equations (8), (9), and (10) yield the electron spectrum obtained in a rigid electrostatic potential $V(z)$, which provides a good agreement with experimental data. We relate this agreement to a large gap Δ_{12} between subbands indicating strong electrostatic potential $V(z)$ in the system. The electron transport depends on the distribution of the quantum levels in the interval kT near the Fermi energy E_F [30]. Below we focus on this part of the spectrum.

Figure 4 presents variations of the electron spectrum with the perpendicular magnetic field in the vicinity of E_F at two different angles α as labeled. Two subbands provide two sets of Landau levels moving at a different rates with $B_\perp$. At $\alpha = 0$ degrees ($B_\parallel = 0$ T) these two sets intersect at the same perpendicular magnetic field, as emphasized by the two vertical dashed lines. These level intersections lead to MISO maxima and correspond to the relation Eq. (1).

At $\alpha = 88$ degrees a finite in-plane is applied. The most apparent transformation the electron spectra is the absence of a coherent intersection of two subbands. In fact at this angle only two levels are intersecting at a given $B_\perp$ in the shown energy interval in the vicinity of E_F. The absence of coherent intersections of Landau levels within the kT interval near E_F leads to a significant reduction of the conductivity σ in Eq. (3), since the two spectra do not overlap well.

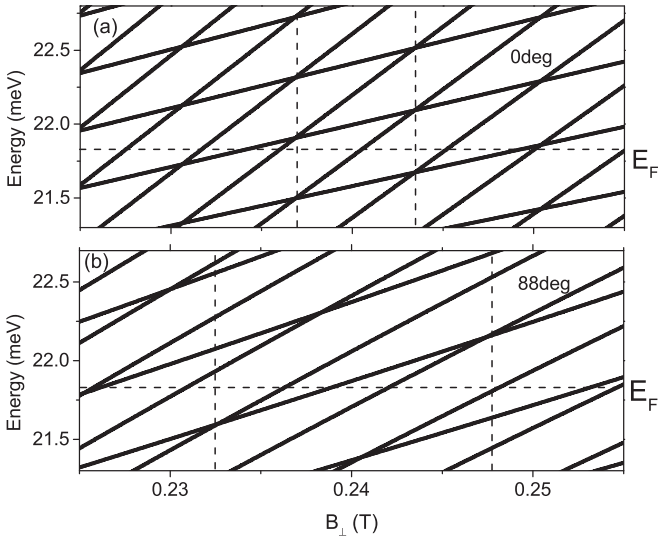

FIG. 4. Panel (a) presents the electron spectrum at $\alpha = 0$ degrees in the vicinity of Fermi energy E_F. Vertical dashed lines indicate that intersections between all subband levels occur at the same magnetic field. Panel (b) presents the electron spectrum at $\alpha = 88$ degrees in which intersections of the quantum levels are not aligned anymore.

Another apparent property of the angular evolution of these spectra is the increase of the interval of the magnetic field between consecutive intersections of a level with the levels in the other subband. This evolution suggests an increase of the MISO period at higher parallel fields. The numerical computations indicate that the main contributions to the level misalignment in tilted magnetic fields are due to the entanglements of the Landau levels via off-diagonal terms described by Eq. (10).

The obtained quantum levels ϵ_i have been split by the Zeeman term, $\Delta_Z = \mu g B$, into two levels ϵ_{is} labeled by spin index $s = \uparrow,\downarrow$ and then broadened by the Gaussian function $G_s(\epsilon) = (m/2\pi\hbar^2)(\omega_c\tau_q)^{1/2}\exp[-(\epsilon - \epsilon_{is})^2/(\hbar^2\omega_c/\pi\tau_q)]$, preserving the degeneracy of the levels [36,37]. The obtained DOS is used in Eqs. (4) and(3) to compute MISO. These numerical computations are compared with experiments in Sec. VI.

V. QPMR IN TILTED MAGNETIC FIELD

In this section we discuss the angular evolution of QPMR in two subband systems. In Fig. 5(a) solid lines represent dependence of normalized QPMR on reciprocal magnetic field, $1/B_\perp$, at different angles α between the direction of the magnetic field and the normal to the sample. Similar to the case of the quantum wells with a single populated subband [15], QPMR is obtained by a subtraction of the magnetoresistance at the critical angle α_c corresponding to the condition $\Delta_Z/\hbar\omega_c = 1/2$ [15,38]. At this condition quantum levels are equally separated by $\hbar\omega_c/2$ and the fundamental harmonic of DOS is absent. At small magnetic fields ($\omega_c\tau_q < 1$) this condition leads to a nearly constant density of states and, thus, the absence of QPMR. In practice in the vicinity of the critical angle the angular variations of the resistance become negligibly small in comparison with the overall angular variation. These small variations limit the accuracy

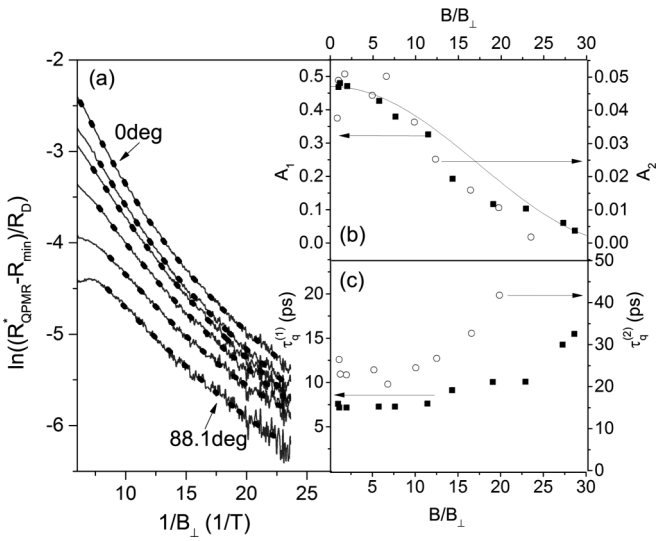

FIG. 5. In panel (a) solid lines present normalized QPMR, $R_{QPMR}/R_D = (R^*_{QPMR} - R_{\min})/R_D$ at different angles. From the top to the bottom $\alpha = 0$, 85, 86, 87, 87.9, and 88.1 degrees. Symbols show theoretical fit to the data using Eq. (11). Panel (b) shows the dependence of the fitting parameters A_i on the ratio $B/B_\perp$, which is compared with the dependence following from Eq. (6) at $g_1 = g_2 = 0.43$. Panel (c) shows dependence of the quantum lifetimes in both subbands on the ratio $B/B_\perp \sim \Delta_Z/\hbar\omega_c$.

at which the QPMR can be obtained at large angles α. In this study we use $\alpha_c = 88.6$ degrees. Shown in Fig. 3(a), the curve at $\alpha_c = 88.6$ degrees is labeled $R_{\min}$ and is related to classical contributions to the magnetoresistance [27,29,30]. The subtraction of $R_{\min}$ from the nonoscillating content of the magnetoresistance yields QPMR: $R_{QPMR} = R^*_{QPMR} - R_{\min}$. A normalized QPMR, R_{QPMR}/R_D, is presented in Fig. 5(a), where R_D is the resistance in zero magnetic field.

Figure 5(a) shows that the decrease of the QPMR with the angle α is considerable and roughly uniform in the reciprocal magnetic field, $1/B_\perp$, indicating a consistent reduction of the cosine functions in Eq. (6) due to the increase of the ratio $\Delta_Z/\hbar\omega_c$ with the angle. At $\alpha = 0$ degrees QPMR follows a curved line, suggesting the presence of two exponential terms expected from Eq. (6), which is rewritten below in the following form:

$$\frac{\sigma_{QPMR}}{\sigma_D} = A_1 \exp\left(-\frac{2\pi}{\omega_c \tau_q^{(1)}}\right) + A_2 \exp\left(-\frac{2\pi}{\omega_c \tau_q^{(2)}}\right), \tag{11}$$

where coefficient $A_i = 2(\sigma_D^{(i)}/\sigma_D)\cos^2[(\pi\Delta_Z^{(i)})/(\hbar\omega_c)]$. Using four fitting parameters A_i and $\tau_q^{(i)}$, we fit the dependences presented in Fig. 5(a) using Eq. (11) and relation $\sigma_{QPMR}/\sigma_D \approx R_{QPMR}/R_D$, which is valid in strong magnetic fields (see Sec. VII).

Figure 5(b) shows the angular dependence of the parameters A_i. Both parameters A_1 and A_2 decrease significantly with the tilt of the magnetic field. The coefficient A_1 is approximately ten times larger than the coefficient A_2 for all angles, leading to the ratio $\sigma_D^{(1)}/\sigma_D^{(2)} \approx 10$. Taking into account the electron density in two bands, $n_{1,(2)} = 6.1(1.87) \times 10^{11}$ cm^{-2}, we have obtained the ratio between transport scattering times: $\tau_{tr}^{(2)}/\tau_{tr}^{(1)} \approx 3$. The data thus indicate three times higher mobility in the upper subband. This mobility increase can be partially related to the reduced carrier velocity, $v_F^{(2)} \sim (n_2)^{1/2}$ in the upper subband, leading to an increase of the mean free time between scattering events: $\tau_{tr} = l_p/v_F$, where l_p is the mean free path.

The decrease of coefficients A_1 and A_2 roughly follows the same dependence, suggesting approximately the same g factor in both subbands. This experimental dependence is close to the dependence expected from Eq. (6) at $\alpha_c = 88.6$ degrees corresponding to $g_{QPMR} = 0.43$, which is represented by the solid line in the figure. The g factor obtained from the angular evolution of MISO (see next section) is $g_{MISO} = 0.15$–0.25. The obtained g factors are close to the bare g factor in GaAs quantum wells [39,40] and significantly smaller the one obtained from QPMR [28] and SdH oscillations [41–43] in GaAs quantum wells with a single populated subband.

Figure 5(c) shows the angular dependence of the quantum scattering times $\tau_q^{(i)}$. The experiments indicate an increase of the quantum scattering time at high angles. We relate this increase to the reduction of the impurity assisted spin flip scattering at high magnetic fields due to the Zeeman splitting of the Landau levels. The observed overall increase of the quantum scattering times approximately by a factor of 2 correlates with the decrease of the density of state by about two times due to the spin splitting of separated Landau levels, that leads to the proportional reduction of the quantum scattering rate [15].

VI. MISO IN TILTED MAGNETIC FIELD

In this section we present a comparison of the angular evolution of MISO shown in Fig. 3(b) with the model. Two MISO properties have been identified: decrease of the MISO amplitude at large angles and variations of the MISO period in tilted magnetic fields. Below we discuss these main properties and indicate an additional MISO property which is not understood.

Figure 6 presents the dependence of MISO period in the reciprocal magnetic field, $1/B_\perp$, on the strength of the parallel magnetic field. Different symbols show the period in the vicinity of different perpendicular magnetic fields as labeled. The experiment demonstrates that the MISO period depends mostly on the strength of the parallel magnetic field. At different $B_\perp$ the dependencies overlap well, indicating no obvious dependence on $B_\perp$. The period is in a good agreement with the numerical computations of the MISO period in tilted magnetic fields at $d = 33$ nm, which is represented by the solid curve in the figure. For a comparison there are two dependencies of the MISO period computed numerically for similar rectangular quantum wells but with other widths: 40 and 20 nm. These dependencies deviate significantly from the experiments.

The obtained width $d = 33$ nm is in a good agreement with the one estimated at $\alpha = 0$ degrees via analytical evaluations of the bottoms of the subband energy spectra. For the rectangular potential well, $V(z)$, used in the model [see Eq. (8)], the eigenfunctions $|0,S\rangle = |0\rangle(2/d)^{1/2}\cos(\pi z/d)$ and $|0,AS\rangle = |0\rangle(2/d)^{1/2}\sin(2\pi z/d)$

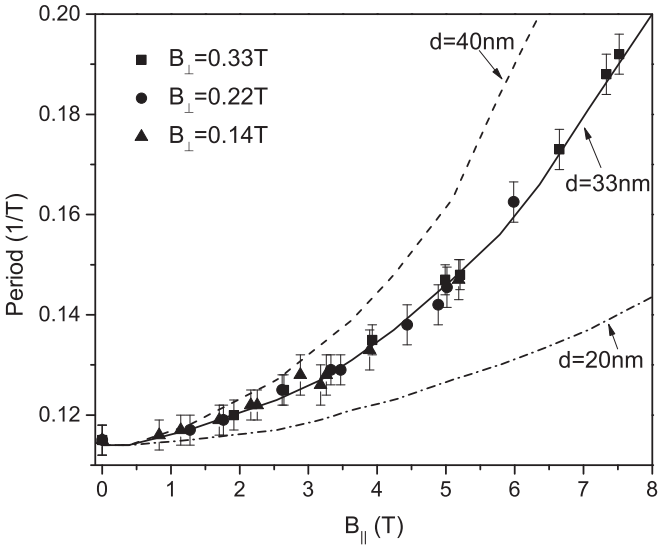

FIG. 6. Symbols present dependence of MISO period in the reciprocal magnetic field, $1/B_\perp$, on the parallel magnetic field taken in the vicinity of different perpendicular magnetic fields as labeled. Lines represent theoretical dependences of the MISO period obtained via numerical computations of the electron spectrum in tilted magnetic fields, using Eq. (8), for different widths d of the quantum well as labeled.

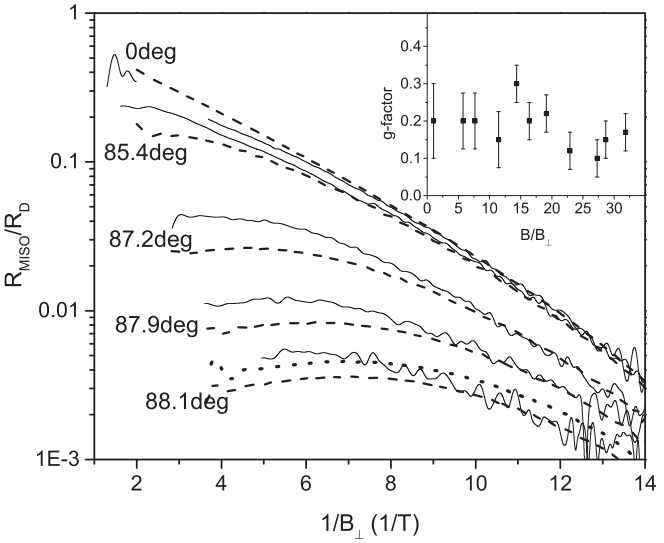

FIG. 7. Solid lines represent normalized swing of MISO at different angles α as labeled. Dashed lines represent theoretical dependencies of the MISO swing on the reciprocal perpendicular magnetic field obtained at the following fitting parameters: $A^*_{MISO} = A_{MISO}A_b = 0.38\cos(0.091/B_\perp)$, $1\tau_q^{(1)} = 1/\tau_q^{(2)} = 125$ GHz, used for all angles and different g factors shown in the inset. The dotted line represents theoretical dependence at $\alpha = 88.1$ degrees, ignoring the Zeeman splitting.

correspond to the eigenvalues $E_1 = \hbar\omega_c/2 + \hbar^2\pi^2/(2m^*d^2)$ and $E_2 = \hbar\omega_c/2 + \hbar^2 4\pi^2/(2m^*d^2)$ at the bottom of the bands, leading to $\Delta_{12} = E_2 - E_1 = (3\pi^2/d^2)(\hbar^2/2m^*)$. This relation yields $d^2 = (3\pi^2 T_{12}/2)(\hbar/e)$, where T_{12} is the MISO period shown in Fig. 6 at $B_\parallel = 0$ T. The last relation yields $d_{th} = 32.6$ nm, which is very close to the $d = 33$ nm obtained in the fitting shown in Fig. 6. We note that the obtained values of the quantum well width are slightly larger than the actual width, $d_0 = 26$ nm, measured during the sample growth. Our experiment suggests that the electron wave function penetrates by about 3 nm into AlAs/GaAs superlattice barriers sandwiching the quantum well.

We have determined that the dominant contribution to the increase of the MISO period is provided by the $B_\parallel$-induced coupling between spatial subbands. This coupling in due to the Lorentz force and is described by the off-diagonal matrix T_{mn} in Eq. (10). Figure 4 indicates that the application of in-plane magnetic field increases the interval between consecutive intersections of a Landau level, which is the major effect leading to the increase of MISO period. The diamagnetic shifts of the subbands [last terms in Eq. (9)] provide subleading contributions, reducing the main effect. In particular, in the absence of the diamagnetic terms, the correspondence shown in the Fig. 6 between the experiment and model occurs at $d = 31$ nm.

Figure 7 presents a dependence of the normalized swing of MISO on the reciprocal magnetic field, $1/B_\perp$, at different angles α as labeled. In accordance with Eq. (7), at $B_\parallel = 0$ T the MISO amplitude is proportional to the product $\delta_1\delta_2$ of Dingle factors in two subbands. In the semilogarithmic scale used in Fig. 7, a straight line should represent this dependence. In contrast, at $\alpha = 0$ degrees the observed dependence deviates significantly from a straight line that has been seen previously [9]. An attractive mechanism, which may lead to these deviations, is a nonparabolic spectrum of 2D electrons due to the presence of the valence band. The nonparabolicity makes the quantized spectrum be not periodic with the energy, leading to a breakdown of the perfect spectral overlap between subbands at MISO maxima described by Eq. (1). This breakdown decreases the MISO amplitude.

Our numerical simulations of MISO in systems with a nonparabolic spectrum indicate good agreement with the experiment at $\alpha = 0$ degrees. However, a considerable disagreement is found in the tilted magnetic field. The numerical simulations indicate that the $B_\parallel$ induced entanglement between nonparabolic subbands leads to a stronger reduction of MISO amplitude than is seen in the experiment.

A better overall agreement is obtained by assuming an additional angular independent beating between two MISO. This beating could be due to a small difference between two masses in two parabolic bands and/or due to fluctuations of the gap Δ_{12} in the quantum well with nonideal boundaries. In this paper we have used the angular independent MISO beating, which is described by a phenomenological amplitude factor, $A_b = \cos(0.091/B_\perp)$. This beating leads to the additional reduction of the normalized MISO amplitude in high reciprocal fields, $1/B_\perp$: $A^*_{MISO} = A_{MISO}A_B$, where $A_{MISO} = 2\sigma_D^{(12)}/\sigma_D$ is normalized Drude factor in Eq. (7).

Figure 7 shows good agreement between experiment and numerical computations of the MISO amplitude at $\alpha = 0$ degrees. The computations use the electron spectrum obtained numerically as described in Sec. IV B. Small angular variations of MISO are observed at $\alpha < 85$ degrees. The largest angular changes in MISO amplitude are found at $\alpha > 85$ degrees. The numerical computations have captured most of the changes,

especially in high reciprocal magnetic fields. The shape of the numerical dependences on $1/B_\perp$ is similar to the one of the experimental curves.

Two main competing factors determine the MISO magnitude in tilted fields. One is the product of the Dingle factors, $\delta_1\delta_2$, decreasing with $1/B_\perp$ in accordance with Eq. (7). Another factor is the misalignment of the intersections of the quantum levels due to the $B_\parallel$-induced entanglement of the levels, which is shown in Fig. 5. The misalignment breaks the perfect spectral overlap between subbands, described by Eq. (1), and leads to a decrease of the MISO amplitude at high $B_\parallel$. A competition between these two mechanisms produces a maximum in MISO amplitude, which can be seen in Fig. 7 at the angle $\alpha = 87.9$ degrees in both experiment and simulation.

The obtained fitting parameters, $A_{MISO} = 0.38$ and $1/\tau_q^{(1)} = 1/\tau_q^{(2)} = 125$ GHz, are quite reasonable. The normalized Drude factor $A_{MISO} = 2\sigma_D^{(12)}/\sigma_D$ indicates about 20% contribution of the effective intersubband scattering to the total Drude conductivity, σ_D, of the 2D system [14]. In accordance with Eq. (7), the sum of the quantum scattering rates in two subbands, $2/\tau_q^{MISO} = 1\tau_q^{(1)} + 1/\tau_q^{(2)} = 250$ GHz, determines the exponential MISO decrease with $1/B_\perp$. This value is in fair agreement with the one obtained in the QPMR analysis and presented in Fig. 5: $2/\tau_q^{QPMR} = 1\tau_q^{(1)} + 1/\tau_q^{(2)} =$ 130–190 GHz.

The Zeeman splitting provides a subdominant contribution leading to a uniform decrease of the MISO amplitude. In Fig. 7 the dotted line represents the numerical simulation neglecting the Zeeman term and the dashed line represents the simulation taking into account the Zeeman contribution at $\alpha = 88.1$ degrees. There is a small vertical displacement between these two curves, indicating that the Zeeman splitting provides a subleading contribution to the overall decrease of MISO amplitude with the tilt of the magnetic field. Using the Zeeman term as a fitting parameter, we have obtained a better agreement between experiment and simulation. The inset in the figure presents the electron g factor extracted from the fit. The obtained g factor is smaller than the one found in QPMR analysis, $g_{qpmr} = 0.4$–0.5, and significantly smaller than the one obtained from transport measurements in quantum wells with a single populated subband [15,42]. The small value of the electron g factor suggests that, in contrast to quantum wells with one subband populated, the exchange interaction contributions to the spin susceptibility are significantly smaller in quantum wells with two populated subbands.

At a small $1/B_\perp$, consistent deviations between the experiment and numerical simulations are evident. The MISO simulations demonstrate a stronger angular decrease than the experiment. The origin of these deviations could be related to a specific shape of the DOS used in the simulations. This issue has not been studied.

VII. CLASSICAL MAGNETORESISTANCE

As presented in the previous sections, the angular evolution of the quantum contributions to the electron conductivity agrees with the semiquantitative model, postulating a strong scattering between spin subbands [15]. We note that this model has not specified any particular relations between

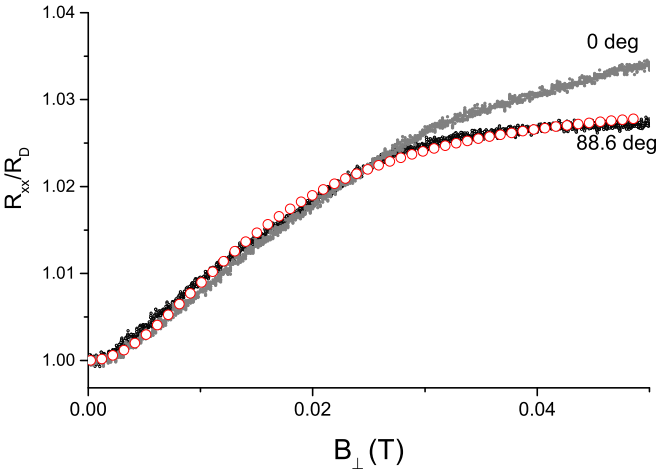

FIG. 8. Dependence of normalized dissipative resistance on the perpendicular component of a magnetic field at two different angles α between the magnetic field and normal to the sample as labeled. Open symbols represent classical magnetoresistance expected from Eq. (12) at $\nu_s = 22.26$ GHz and $\nu_r = 41$ GHz.

coefficients $\sigma_D^{(1)}$, $\sigma_D^{(2)}$, and $\sigma_D^{(12)}$ in Eq. (4). This section presents a quantitative comparison of our results with the existing quantitative theory of the magnetoresistance in the perpendicular magnetic field ($\alpha = 0$ degrees) [13,14,25,29]. Below we have found that QPMR and the classical magnetoresistance agree quantitatively with the theory. An inclusion of MISO into the consideration leads to a significant quantitative disagreement between the experiment and the theory.

At $B_\perp < 0.03$ T the magnetoresistance presented in Fig. 2 demonstrates a few percent increase with the magnetic field, which is independent of the in-plane magnetic field. Figure 8 shows this part of the magnetoresistance in detail for two angles as labeled. The experiment indicates that at high tilt of the magnetic field ($\alpha = 88.6$ degrees), at which the modulation of the electron spectrum is suppressed by the Zeeman splitting of Landau levels, the magnetoresistance saturates above 0.03 T. At $\alpha = 0$ degrees the magnetoresistance shows a tendency to the saturation. The two dependencies deviate from each other at $B_\perp > 0.03$ T, indicating the presence of QPMR. At $B_\perp <$ 0.03 T two dependencies coincide, suggesting the absence of DOS modulations. The increase at small magnetic fields is related to the classical magnetoresistance expected in electron systems with several subbands populated [29,30].

The mechanism of the classical positive magnetoresistance (CMR) is similar to that for two groups of carriers with different mobilities [30]. However, in a two-subband system, due to the intersubband coupling via scattering, the classical resistivity $\rho_{\rm class}$ is not reduced simply to the contribution given by two independent groups of carriers from the first and second subbands [29]. The classical resistivity can be conveniently presented as [26]

$$\rho_{\rm class} = \frac{m}{e^2 n}\frac{\omega_c^2\nu_s + \nu_*\nu_r^2}{\omega_c^2 + \nu_r^2}, \qquad (12)$$

where $n = n_1 + n_2$ is the total electron density and n_1 and n_2 are the electron densities in the subbands. This contribution increases with the magnetic field, starting from the zero-field value $\rho_D = m\nu_*/e^2 n$, and saturates at $\omega_c \gg \nu_s$ with the value

$\rho_{sat} = m\nu_s/e^2 n$. The characteristic rates ν_s, ν_r, and ν_* are given by

$$\begin{aligned}\nu_s &= (n_1/n)\nu_{11}^{tr} + (n_2/n)\nu_{22}^{tr} + \nu_{12}^{tr},\\ \nu_r &= (n_2/n)\nu_{11}^{tr} + (n_1/n)\nu_{22}^{tr} + 2\nu_{12} - \nu_{12}^{tr},\\ \nu_* &= \frac{\left(\nu_{11}^{tr}+\nu_{12}\right)\left(\nu_{22}^{tr}+\nu_{12}\right) - \left(\nu_{12}-\nu_{12}^{tr}\right)^2 n^2/4n_1n_2}{\nu_r}, \quad (13)\end{aligned}$$

where ν_{ij} (ν_{ij}^{tr}) are quantum (transport) scattering rates [14].

In small quantizing magnetic fields, $\omega_c\tau_q^{(i)} < 1$, the QPMR and MISO can be presented as [14,26]

$$\begin{aligned}\rho_{QPMR} &= \frac{2m}{e^2 n}\left[\frac{n_1}{n}\nu_{11}^{tr}e^{-2\alpha_1} + \frac{n_2}{n}\nu_{22}^{tr}e^{-2\alpha_2}\right],\\ \rho_{MISO} &= \frac{2m}{e^2 n}\left[\nu_{12}^{tr}e^{-\alpha_1-\alpha_2}\cos\frac{2\pi\,\Delta_{12}}{\hbar\omega_c}\right], \quad (14)\end{aligned}$$

where $\alpha_i = \pi/(\omega_c\tau_q^{(i)}) = \pi(\nu_{ii}+\nu_{12})/\omega_c$ are the Dingle exponents.

In Fig. 8 the open symbols present the normalized classical magnetoresistance coming from Eq. (12). The figure indicates a good agreement between experiment at $\alpha = 88.6$ degrees and the theory. The fit yields two parameters: the scattering rate in classically strong magnetic fields $\nu_s = 22.26 \pm 0.03$ GHz and $\nu_r = 41 \pm 0.03$ GHz. The value of the resistivity at $B = 0$ T yields the scattering rate at zero magnetic field, $\nu_* = 21.6 \pm 0.02$ GHz. Equation (14) provides a quantitative relation between coefficients A_i used to fit QPMR [see Eq. (11)]: $A_i = (2n_1/n)(\nu_{ii}^{tr}/\nu_*)$, yielding $\nu_{11}^{tr} = 7.05$ GHz and $\nu_{22}^{tr} = 2.3$ GHz. A substitution of these values into the relation for ν_s in Eq. (13) yields the intersubband scattering rate, $\nu_{12}^{tr} = 16.32$ GHz. The substitution of the obtained transport scattering rates into the relation for ν_r in Eq.(13) leads to the intersubband quantum scattering rate, $\nu_{12} = 26.95$ GHz. The intrasubband quantum scattering rates ν_{ii} now can be found from the total quantum scattering rates, $1/\tau_q^{(i)} = \nu_{ii} + \nu_{12}$, obtained from the comparison of QPMR with Eq. (14) and presented in Fig. 5. The intrasubband rates are found to be $\nu_{11} = 106$ GHz and $\nu_{22} = 18$ GHz. Using the obtained scattering rates, we have computed the total scattering rate ν_* expected from Eq. (13) at zero magnetic field, $\nu_*^{th} = 20.4$ GHz, which is close to one seen in the experiment, $\nu_* = 21.6$ GHz. Thus the cross-comparison of QPMR, CMR, and the theory indicates a good mutual agreement.

The comparison of QPMR and CMR demonstrates the dominant contribution of the intersubband scattering to the electron transport. Indeed the intersubband transport scattering rate, $\nu_{12}^{tr} = 16.3$ GHz, is the main part of the total transport scattering rate, $\nu_s = 22.26$ GHz, of electrons in strong magnetic fields. This can be related to the fact that, in contrast to the quantum intrasubband scattering leading to a small displacement of the cyclotron orbit in the studied system, any intersubband quantum scattering event leads to a significant ($\sim R_c^{(1)}$) displacement of the center of the electron orbit resulting in a high dissipative conductivity. The large orbital displacement is due to the substantial difference in the cyclotron radii $R_c^{(i)}$ of electrons at Fermi energy in two subbands with very different electron densities. This observation is in agreement with the obtained result: $\nu_{12} \approx \nu_{12}^{tr}$. Furthermore, in the limit where intersubband scattering dominates, $\nu_{12} \approx \nu_{12}^{tr} \gg \nu_{ii}^{tr}$, the total transport scattering rate in strong magnetic fields, $\nu_s \approx \nu_{12}^{tr}$, is close to the total scattering rate at zero magnetic field, $\nu_* \approx (\nu_{12})^2/\nu_r \approx \nu_{12}$, in the agreement with the experiment. Indeed Fig. 8 demonstrates that the classical magnetoresistance is weak (about 3 percent variation) despite the large difference in the intrasubband scattering rates ν_{ii}^{tr}.

An inclusion of MISO in the consideration destroys the obtained agreement. The comparison of the MISO amplitude with the theory, which is presented in Fig. 7, yields $A_{MISO} \approx 0.38$, leading, in accordance with Eq. (14), to the intersubband transport scattering rate $\nu_{MISO}^{tr} \approx 4.2$ GHz. The obtained value is about four times less that the ν_{12}^{tr} found via analysis of QPMR and CMR. In contrast, the sum of the total quantum scattering rates obtained from the MISO analysis, $\nu_{MISO} = 1/\tau_q^{(1)} + 1/\tau_q^{(2)} \approx 250$ GHz (see the caption of Fig. 7) agrees reasonably well with the one obtained from QPMR: $\nu_{QPMR} \approx 133 + 45 = 178$ GHz (see Fig. 5).

The observed strong quantitative discrepancy in MISO amplitude suggest that some scattering processes may not been taken correctly in the theoretical consideration of MISO. In particular, recent experiments on QPMR in tilted magnetic fields [15] indicate the importance of spin flip processes (spin mixing) in the studied 2D systems. Such processes are ignored by the existing quantitative theory. While the spin mixing seems to be not important for QPMR in the perpendicular magnetic field [15], the magnitude of MISO may have substantial dependence on the spin mixing between different spatial subbands. In particular, if we assume that the spin mixing between spatial subbands is absent then the magnitude of MISO in Eq. (7) should be reduced by factor of 2. This follows from the replacement of the products of the total density of states $\nu_1\nu_2 = (\nu_{1\uparrow}+\nu_{1\downarrow})(\nu_{2\uparrow}+\nu_{2\downarrow})$ in Eq. (3) by $\nu_{1\uparrow}\nu_{2\uparrow} + \nu_{1\downarrow}\nu_{2\downarrow}$ corresponding to the absence of the spin flip intersubband scattering.

VIII. SUMMARY

Quantum positive magnetoresistance (QPMR) and magneto-intersubband resistance oscillations (MISO) of highly mobile 2D electrons in symmetric GaAs quantum wells with two populated subbands have been studied in tilted magnetic fields. In the perpendicular magnetic field QPMR displays contributions from two subbands with considerably different electron quantum lifetimes and intrasubband mobilities. MISO evolution with $B_\perp$ agrees with the obtained quantum scattering times only if an extra reduction of the MISO magnitude is applied at small magnetic fields. This indicates the presence of an additional mechanism leading to the MISO damping. A weakly nonparabolic electron spectrum provides a MISO damping, which is comparable to the one seen in the experiments at $\alpha = 0$ degree. A simple beating of two MISOs provides a similar result but fits better the experiments in tilted magnetic fields.

Application of the in-plane magnetic field produces a strong decrease of both QPMR and MISO magnitude. The reduction of QPMR is explained by the spin splitting of Landau levels indicating a g factor, $g_{QPMR} \approx 0.4$–0.5, which

is considerably less than the g factor found in a GaAs quantum well with a single subband populated. In contrast to QPMR, the decrease of MISO magnitude is largely related to the in-plane magnetic field induced entanglement between quantum levels in different subbands that, in addition, increases the MISO period. Zeeman spin splitting provides a subleading contribution to the MISO decrease, indicating an even smaller g factor: $g_{MISO} \approx 0.2$.

Cross comparison of the classical magnetoresistance and QPMR in perpendicular magnetic fields with existing quantitative theory indicates good mutual agreement. The MISO amplitude is found to be significantly less than the one expected from the theory. Taking into account the recent findings [15], which indicate the importance of spin mixing (spin flip scattering) in the studied systems, we suggest that spin degrees of freedom, which are ignored by the existing theory, are relevant for MISO.

ACKNOWLEDGMENTS

The authors thank A. I. Toropov and A. K. Bakarov for the growth of quantum wells. This work was supported by the National Science Foundation (Division of Material Research, 1104503) and the CUNY Bridge Program.

[1] D. Shoenberg, *Magnetic Oscillations in Metals* (Cambridge University Press, New York, 1984).
[2] T. Ando, A. B. Fowler, and F. Stern, Rev. Mod. Phys. B **54**, 437 (1982).
[3] *Spin Physics in Semiconductors*, edited by M. I. Dyakonov (Springer-Verlag, Berlin, 2008).
[4] S. D. Sarma and A. Pinczuk, *Perspectives in Quantum Hall Effects* (Wiley-VCH, Weinheim, 2004).
[5] P. T. Coleridge, Semicond. Sci. Technol. **5**, 961 (1990).
[6] D. R. Leadley, R. Fletcher, R. J. Nicholas, F. Tao, C. T. Foxon, and J. J. Harris, Phys. Rev. B **46**, 12439 (1992).
[7] A. Bykov, D. R. Islamov, A. V. Goran, and A. I. Toropov, JETP Lett. **87**, 477 (2008).
[8] N. C. Mamani, G. M. Gusev, T. E. Lamas, A. K. Bakarov, and O. E. Raichev, Phys. Rev. B **77**, 205327 (2008).
[9] A. V. Goran, A. A. Bykov, A. I. Toropov, and S. A. Vitkalov, Phys. Rev B **80**, 193305 (2009).
[10] A. A. Bykov, A. V. Goran, and S. A. Vitkalov, Phys. Rev. B **81**, 155322 (2010).
[11] L. I. Magarill and A. A. Romanov, Fiz. Tverd. Tela **13**, 993 (1971) [Sov. Phys. Solid State **13**, 828 (1971)].
[12] V. M. Polyanovskii, Fiz. Tekh. Poluprovodn. **22**, 2230 (1988) [Sov. Phys. Semicond. **22**, 1408 (1988)].
[13] M. E. Raikh and T. V. Shahbazyan, Phys. Rev. B **49**, 5531 (1994).
[14] O. E. Raichev, Phys. Rev. B **78**, 125304 (2008).
[15] W. Mayer, J. Kanter, J. Shabani, S. Vitkalov, A. K. Bakarov, and A. A. Bykov, Phys. Rev. B **93**, 115309 (2016).
[16] M. G. Priestley, Proc. R. Soc. London A **276**, 258 (1963).
[17] M. H. Cohen and L. Falicov, Phys. Rev. Lett. **7**, 231 (1961).
[18] E. I. Blount, Phys. Rev. **126**, 1636 (1962).
[19] A. A. Slutskin, Sov. Phys. JETP **26**, 474 (1968).
[20] A. B. Pippard, Proc. R. Soc. London A **270**, 1 (1962).
[21] A. B. Pippard, Philos. Trans. R. Soc. London A **256**, 317 (1964).
[22] J. Hu and A. H. MacDonald, Phys. Rev. B **46**, 12554 (1992).
[23] N. E. Harff, J. A. Simmons, S. K. Lyo, and J. F. Klem, G. S. Boebinger, L. N. Pfeiffer, and K. W. West, Phys. Rev. B **55**, R13405 (1997).
[24] M. A. Mueed, D. Kamburov, M. Shayegan, L. N. Pfeiffer, K. W. West, K. W. Baldwin, and R. Winkler, Phys. Rev. Lett. **114**, 236404 (2015).
[25] M. G. Vavilov and I. L. Aleiner, Phys. Rev. B **69**, 035303 (2004).
[26] N. C. Mamani, G. M. Gusev, E. C. F. da Silva, O. E. Raichev, A. A. Quivy, and A. K. Bakarov, Phys. Rev. B **80**, 085304 (2009).
[27] Scott Dietrich, Sergey Vitkalov, D. V. Dmitriev, and A. A. Bykov, Phys. Rev. B **85**, 115312 (2012).
[28] W. Mayer, A. Ghazaryan, P. Ghaemi, S. Vitkalov, and A. A. Bykov, Phys. Rev. B **94**, 195312 (2016).
[29] E. Zaremba, Phys. Rev. B **45**, 14143 (1992).
[30] J. M. Ziman, *Principles of the Theory of Solids* (Cambridge University Press, Cambridge, 1972).
[31] R. Fletcher, M. Tsaousidou, T. Smith, P. T. Coleridge, Z. R. Wasilewski, and Y. Feng, Phys. Rev. B **71**, 155310 (2005).
[32] D. V. Dmitriev, I. S. Strygin, A. A. Bykov, S. Dietrich, and S. A. Vitkalov, JETP Lett. **95**, 420 (2012).
[33] S. A. Vitkalov, H. Zheng, K. M. Mertes, M. P. Sarachik, and T. M. Klapwijk, Phys. Rev. Lett. **85**, 2164 (2000).
[34] S. A. Vitkalov, H. Zheng, K. M. Mertes, M. P. Sarachik, and T. M. Klapwijk, Phys. Rev. B **63**, 193304 (2001).
[35] S. A. Vitkalov, Phys. Rev. B **64**, 195336 (2001).
[36] M. E. Raikh and T. V. Shahbazyan, Phys. Rev. B **47**, 1522 (1993).
[37] J. Q. Zhang, S. Vitkalov, and A. A. Bykov, Phys. Rev. B **80**, 045310 (2009).
[38] F. F. Fang and P. J. Stiles, Phys. Rev. **174**, 823 (1968).
[39] D. Stein, K. V. Klitzing, and G. Weimann, Phys. Rev. Lett. **51**, 130 (1983).
[40] Yu. A. Nefyodov, A. V. Shchepetilnikov, I. V. Kukushkin, W. Dietsche, and S. Schmult, Phys. Rev. B **83**, 041307(R) (2011).
[41] R. J. Nicholas, R. J. Haug, K. V. Klitzing, and G. Weimann, Phys. Rev. B **37**, 1294 (1988).
[42] D. R. Leadley, R. J. Nicholas, J. J. Harris, and C. T. Foxon, Phys. Rev. B **58**, 13036 (1998).
[43] B. A. Piot, D. K. Maude, M. Henini, Z. R. Wasilewski, J. A. Gupta *et al.*, Phys. Rev. B **75**, 155332 (2007).